Eur Biophys J (2010) 39:959–970
DOI 10.1007/s00249-009-0462-9

ORIGINAL PAPER

An XAS study of the sulfur environment in human neuromelanin and its synthetic analogs

Pier Raimondo Crippa · Melvin Eisner · Silvia Morante · Francesco Stellato · Flavio C. Vicentin · Luigi Zecca

Received: 26 January 2009 / Revised: 9 April 2009 / Accepted: 20 April 2009 / Published online: 27 May 2009

Abstract Neuromelanin is a complex molecule accumulating in the catecholaminergic neurons that undergo a degenerative process in Parkinson's disease. It has been shown to play either a protective or a toxic role depending on whether it is present in the intraneuronal or extraneuronal milieu. Understanding its structure and synthesis mechanisms is mandatory to clarify the reason for this remarkable dual behavior. In the present study, X-ray absorption spectroscopy is employed to investigate the sulfur binding mode in natural human neuromelanin, synthetic neuromelanins, and in certain structurally known model compounds, namely cysteine and decarboxytrichochrome C. Based on comparative fits of human and synthetic neuromelanin spectra in terms of those of model compounds, the occurrence of both cysteine- and trichochrome-like sulfur coordination modes is recognized, and the relative abundance of these two types of structural arrangement is determined. Data on the amount of cysteine- and trichochrome-like sulfur measured in this way indicate that among the synthetic neuromelanins those produced by enzymatic oxidation are the most similar ones to natural neuromelanin. The interest of the method described here lies in the fact that it allows the identification of different sulfur coordination environments in a physically nondestructive way.

Keywords Melanin structure · XANES · Parkinson's disease · Cysteine

Abbreviations

DAC	Auto-oxidation of dopamine and cysteine
DEC	Enzymatic oxidation of dopamine and cysteine
DOPEC	L-DOPA and cysteine enzymatic oxidation
EDTA	Ethylenediaminetetraacetic acid
EXAFS	Extended X-ray absorption fine structure
NM	Neuromelanin
PD	Parkinson's disease
TEY	Total electron yield
XAS	X-ray absorption spectroscopy
XANES	X-ray absorption near edge structure

Introduction

Neuromelanin is a complex, insoluble polymeric pigment present in neurons from different brain regions of several animal species, including humans (for a review see Zucca et al. 2004). Neuromelanin is found in the highest concentration in catecholaminergic neurons of substantia nigra and

Proceedings of the XIX Congress of the Italian Society of Pure and Applied Biophysics (SIBPA), Rome, September 2008.

P. R. Crippa (✉)
Università degli Studi di Parma, V. le G.P. Usberti, 7/A, Parma 43100, Italy
e-mail: pierraimondo.crippa@fis.unipr.it

M. Eisner
University of Houston, 4800 Calhoun Road, Houston, TX 77004, USA

S. Morante · F. Stellato
Università di Roma "Tor Vergata", INFN, SOFT, Via della Ricerca Scientifica, 1, Rome 00133, Italy

F. C. Vicentin
Laboratorio Nacional de Luz Síncrotron, Rua Giuseppe Máximo Scolfaro, 10000, Campinas, SP CEP 13083-100, Brazil

L. Zecca
Institute of Biomedical Technologies-CNR, Via Fratelli Cervi, 93, Segrate (MI) 20090, Italy

locus coeruleus regions of human midbrain (Bogerts 1981; Graham 1989; Zecca et al. 2004). In Parkinson's disease (PD), the concentration of neuromelanin decreases rapidly as pigmented dopaminergic neurons are selectively lost, while nonpigmented neurons are mostly spared (Kastner et al. 1992). It was suggested that neuromelanin can play either a protective or a toxic role with respect to the degeneration of nigral dopamine neurons depending on cellular context (Zecca et al. 2003). Neuromelanin has been proposed to be neuroprotective against toxic metals (Zecca et al. 1994), pesticides (Lindquist et al. 1998), betacarbolines (Östergren et al. 2004), and other toxins, such as 1-methyl-4-phenylpyridinium ion (D'Amato et al. 1986). Moreover, neuromelanin synthesis was considered to provide a neuronal protective function since it prevents the accumulation of cytosolic dopamine (Sulzer et al. 2000). On the other hand, neuromelanin was shown to induce neurotoxicity by overactivation of microglia (Wilms et al. 2003) and inhibition of proteasome (Shamoto-Nagai et al. 2004).

In the neuromelanin molecule, a peptide and a lipid component are present in addition to the melanic component (Zucca et al. 2004, 1992, 2000). The peptide component of neuromelanin amounts to 15% of its weight (Zecca et al. 2000) and cysteine about 0.5%. The melanic component is composed of two classes of molecules in rather well-determined proportions. One is a benzothiazine-based molecule characteristic of pheomelanin that is formed through the incorporation of cysteine with dopamine; it constitutes 20–25% of the total melanic component of human neuromelanin. The other one is an indole-based molecule characteristic of eumelanin that is formed through the oxidation of dopamine (Odh et al. 1994; Wakamatsu et al. 2003). The identification of dopamine and cysteinyl-dopamine as building blocks of natural neuromelanin lends support to the idea that its synthesis plays a detoxifying role, preventing an otherwise toxic intraneuronal accumulation of dopamine compounds (Sulzer et al. 2000; Wakamatsu et al. 2003).

X-ray diffraction studies (Crippa et al. 1996) have shown that neuromelanin has a multilayer (graphite-like) three-dimensional structure made of planar overlapping sheets of molecules containing indolebenzothiazine rings (Zecca et al. 2000). This structure appears to be similar to what was first proposed by Chio (1976) for synthetic L-DOPA melanin and investigated in more detail in Cheng et al. (1994) where the study was extended to the case of natural *Sepia* eumelanin.

Scanning probe and photoelectron emission microscopies have demonstrated that neuromelanin granules are comprised of spherical structures with a diameter of ~30 nm with pheomelanin at the core and eumelanin at the surface (Bush et al. 2006).

As for the sulfur (S) geometries in neuromelanin, chemical degradation methods have shown that S is present in two different structures (coordination modes), namely bound in cysteine- and benzothiazine-like environments (Wakamatsu et al. 2003; Zecca et al. 2000). We recall that the S group (–C–S–H) present in cysteine and the benzothiazine structure (–C–S–C–) present in trichochrome differ in their electronic configuration around S essentially as a consequence of the differences in the electronegativity of the –S–H and –S–C– bonds.

A detailed characterization of the neuromelanin structure is still lacking and would represent an essential step in understanding neuromelanin's synthesis, interaction with other neuronal-glial compounds, its metabolic fate, and role in normal aging and PD neurodegenerative processes. In addition, a direct (i.e., spectroscopic) demonstration of the presence of S in heterocyclic thiazine- and cysteine-like structures in natural neuromelanin is also missing.

In this work, we exploit the presence of S as the absorbing center for X-ray absorption spectroscopy (XAS) experiments with the purpose of settling the last issue. Due to its chemical selectivity and sensitivity to the local atomic arrangement, XAS is in fact the technique of election for structural studies on biological materials when one wants to characterize the atomic structure around a given absorber.

Spectra in the X-ray absorption near edge structure (XANES) region around the S absorption K-edge of natural and synthetic melanins, as well as of two S-containing model compounds have been measured at the Brazilian Synchrotron Light Laboratory (http://www.lnls.br/lnls/cgi/cgilua.exe/sys/start.htm?tpl=home).

The two model compounds, namely decarboxytrichochrome C and cysteine, whose structures are shown in Fig. 1a and b, respectively, have been subjected to XAS measurements because they represent prototypes of

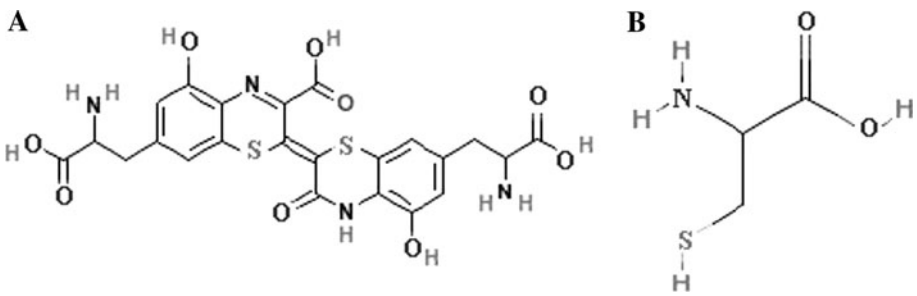

Fig. 1 Chemical composition of **a** decarboxytrichochrome C and **b** cysteine residue

different chemical structures in which S can be found. In cysteine, in fact, where aromatic rings are not present, the unique S is bound to light atoms. In decarboxytrichochrome C, in contrast, two S atoms are present and are both part of aromatic rings.

As the structure of these model compounds is known, the characteristic features of their XANES spectrum can be used as fingerprints for the presence of well-defined S atomic environments in natural neuromelanin, much in the spirit of what has been done in the case of other absorbing centers (Meneghini and Morante 1998; Morante 2001; Morante et al. 2004).

Experimental methods

Sample preparation

The samples subjected to XAS measurements in this investigation can be divided into three groups, namely natural neuromelanin, synthetic neuromelanins, and model compounds. They have been prepared or isolated according to the following protocols.

Natural neuromelanin

Natural neuromelanin was isolated from cerebellum as described in (Zecca et al. 2002). We will refer to it as NM in the rest of this paper. An aliquot of 3.0 g brain tissue was introduced into a 130-ml plastic centrifuge tube. After grinding, 90 ml water was added, and the mixture was shaken. Tubes were centrifuged at 18,000×*g* for 15 min, and the pellet was washed twice with 90 ml phosphate buffer (50 mM, pH 7.4). The sample was then incubated for 3 h at +37°C with 60 ml Tris buffer (50 mM, pH 7.4) containing sodium dodecyl sulfate (5 mg/ml) and L-cysteine (15 mM). This suspension was centrifuged at 18,000×*g* for 20 min, the supernatant removed, and the pellet incubated for 3 h at +37°C with 20 ml of the same solution. The pigment was separated by centrifugation as above, washed twice with 5 ml NaCl solution (9 mg/ml), and washed with 3 ml water. The sample was suspended in 2 ml methanol, centrifuged, and the supernatant fluid removed. The sample was resuspended in 1 ml hexane, centrifuged, and after eliminating the supernatant fluid, the pigment was dried under nitrogen flow and placed in vacuum for 14 h.

Synthetic neuromelanins

DAC The synthetic melanin obtained from auto-oxidation of dopamine and cysteine (DAC for short in the rest of this paper) was prepared (Zecca et al. 2000) so as to try to best reproduce the chemical composition of NM, particularly in relation to its S content. To this end dopamine (1.96 mmol) and cysteine (0.03 mmol) were dissolved in a flask containing 200 ml of 0.05 M sodium phosphate buffer (pH 7.4). The solution, protected from light, was allowed to auto-oxidize in air at +37°C. After 108 h, the suspension was centrifuged (10,000 rpm for 10 min), and 200 ml of freshly prepared phosphate buffer containing 0.03 mmol of cysteine was added to the melanin sample obtained in this way. The reaction was continued for another 24 h, and at the end, the resulting brown suspension was transferred into centrifuge glass tubes and centrifuged (10,000 rpm for 10 min). The precipitated melanin was resuspended in 5 ml of 1% acetic acid, centrifuged, and washed with 5 ml of water. Then, it was reacted twice with 0.15 M Na_2 EDTA and washed twice with water. The synthetic melanin was dialyzed in order to remove salts and other low-molecular-weight substances. After drying as described above, the final yield was 30% of the initial amount of dopamine.

DEC The synthetic melanin produced from enzymatic oxidation of dopamine and cysteine (DEC for short in the rest of this paper) was prepared (Zecca et al. 1996) as follows. An amount of 0.39 mmol of dopamine was dissolved into a flask containing 200 ml of 0.05 M sodium phosphate buffer (pH 7.4), together with 61 mg of cysteine and 7 mg of tyrosinase (EC 1.14.18.1, Sigma, St. Louis, MO, USA). The solution was left to react at +37°C for 90 h. Then the reaction was stopped by decreasing the pH to 3.0 with 30% acetic acid. The suspension was transferred into glass tubes and centrifuged (10,000 rpm for 10 min) at +25°C. The precipitate of melanin was resuspended in 7 ml of 0.05 M Tris buffer (pH 7.4) containing 5 mg/ml of sodium dodecylsulfate and allowed to incubate at +37°C for 2 h. Then it was washed with 10 ml of NaC1 (9 mg/ml), and after centrifugation, the melanin was reacted twice with 20 ml of 0.15 M Na_2 EDTA for 8 h, in order to remove every trace of metals. The suspension was centrifuged, and the precipitate washed twice with 10 ml water. Finally, it was washed with acetone and dried as described above. The final yield was 47% of the initial amount of dopamine.

DOPEC The synthetic melanin from L-DOPA and cysteine enzymatic oxidation (DOPEC for short in the rest of the paper) is prepared according to the following procedure. Tyrosinase (10 mg) was added to a stirred solution containing 0.51 mmol of L-DOPA in 100 ml phosphate buffer 0.05 M at pH 7. After 30 s, 1.0 mmol of L-cysteine dissolved in the same buffer was added, and after 24 h the solution was made acidic (pH 3.5) by HCl. The precipitate, collected by centrifugation, was washed three times with a

pH 3.5 HCl solution and then with acetone. Finally, it was dried as described above.

Model compounds

Decarboxytrichochrome C (96%) was a kind gift by Prof. S. Ito and was prepared as described by Ye et al. (2003). Finally cysteine (98%) was bought from Sigma–Aldrich and used without further purification.

Data collection

XAS data at the S K-edge have been collected at the D04B bending magnet beam line of the Brazilian Synchrotron Light Laboratory. A Si (111) double crystal monochromator was used throughout the study. X-ray spectra were recorded in total electron yield (TEY) mode by collecting the sample drain current, I_{TEY}, with an electrometer (Keithley 617). TEY detection method instead of transmission has been chosen because of the high sample absorption in this energy range. It is well known (Ebel 2004), in fact, that the probability of emission of Auger electrons, which provides the main contribution to the total yield signal, increases with decreasing atomic number of the absorbing atom. Before hitting the sample, the beam goes through a 0.75-μm sheet of aluminum foil in order to measure the "impinging" drain current, I_0.

It can be shown that in TEY detection, the ratio I_{TEY}/I_0 is to a good approximation proportional to the absorption coefficient, μ (Heald 1988).

Unfortunately in this investigation we have to limit our analysis to the XANES region of the spectrum, i.e., to an energy interval around the edge not larger than about 20 eV, because for higher energies, where the extended X-ray absorption fine structure (EXAFS) region starts, the recorded signal is essentially flat. There is a number of possible concurrent reasons that can be called upon to explain the absence of EXAFS oscillations in the measured spectra. First of all, it should be recalled that the amplitude of the oscillations of the signal decreases monotonically with energy in the EXAFS region (Backnaes et al. 2008; Fleet 2005) in a way that depends on the absorber and that is especially fast for light absorbers, such as S (Stöhr et al. 1994). A second reason is that the TEY detection method, when used in experiments with insulating specimens as in our case, suffers from charging problems (Vlachos et al. 2005). This feature tends to significantly reduce the intensity of the collected signal (Gilbert et al. 2000) at large energies (i.e., in the EXAFS region). Finally, and perhaps most importantly, we are dealing with samples where the absorber lives in a particularly disordered environment.

In conclusion, as a result of these adverse circumstances and inherent difficulties, we have been forced to limit our investigation to the consideration of only the XANES part of the collected spectra.

Data handling

In order to make the available raw spectral data ready for a sensible comparative analysis among different samples, we had to make three kinds of "maneuvers" on the experimental points. First of all, in order to get rid of a number of spurious background contributions affecting the shape of the spectrum, a suitable background subtraction procedure was applied. Secondly, to make possible the type of comparison we want to make in this paper, a normalization procedure for the subtracted spectra is necessary because data have been taken on samples with different and to a large extent unknown S concentrations. Thirdly, the edge energies of the various spectra have to be appropriately matched in order to correct for the visible systematic error in the beam energy calibration.

First step

The first step is very easily accomplished by subtracting from XAS spectral data a linear term fitted through the pre-edge data points.

Second step

The normalization of data to unit S concentration is a much more delicate step as the energy range of the available data beyond the XANES region is very short. This fact prevents us from employing the standard normalization procedure (Ravel and Newville 2005) which, we recall, consists of the following three steps.

A1. The pre-edge region is fitted with a straight line, which is then extrapolated forward, past the edge energy, E_0. (The edge energy E_0 is conventionally defined as the energy where the first derivative of the spectrum has its maximum). We call $\mu_1(E_0)$ the value of the fitted straight line evaluated at E_0.

A2. The post-edge region is fitted with a (low degree) polynomial and extrapolated backward, past the edge energy. We call $\mu_2(E_0)$ the value of the fitted polynomial evaluated at E_0.

A3. The difference $\delta = \mu_1(E_0) - \mu_2(E_0)$ is computed.

In the standard approach, the term in step A1 gives the background contribution to the measured absorption coefficient, while the term in step A2 is identified with the contribution of the isolated absorber to the signal. Therefore, δ is proportional to the absorber concentration and can be used to normalize structurally different samples of the same absorber.

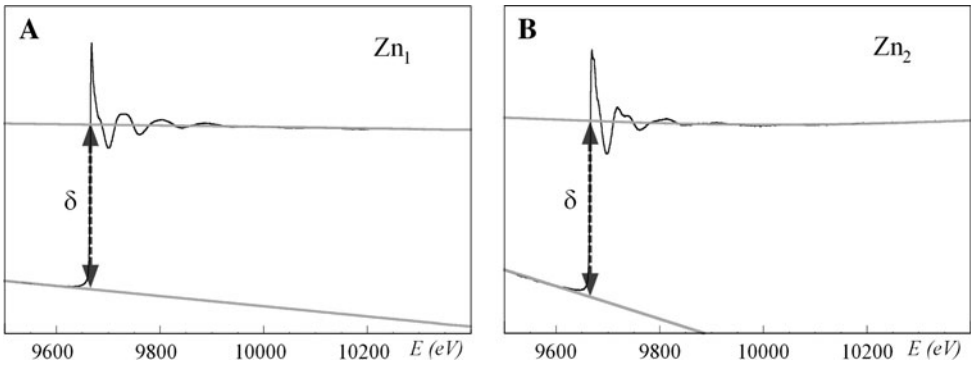

Fig. 2 The standard procedure to compute the edge jump (*line with arrowheads*) in the two representative spectra of the Aβ_{1-40} peptide complexed with Zn is graphically illustrated (**a** Zn_1, **b** Zn_2). Pre-edge and post-edge fit results are drawn in *gray*, superimposed on the experimental data (*black line*)

For illustration we graphically display in Fig. 2 the procedure described above in a situation where good EXAFS data are available. The data we consider are taken from Stellato et al. (2006) and refer to the XAS spectra of the Aβ_{1-40} peptide complexed with Zn, taken at Zn K-edge in two different preparations (Zn_1 and Zn_2 in the following[1]).

Going through steps A1–A3, one finds

$$\delta(Zn_1) = 0.1506, \quad \delta(Zn_2) = 0.0644. \tag{1}$$

Since, as recalled above, δ is proportional to the absorber concentration, one can estimate the sample concentration ratio from the simple formula:

$$\alpha = \delta(Zn_1)/\delta(Zn_2) = 2.34. \tag{2}$$

Within the margin of error, the same number is found by directly comparing the measured numbers of counts obtained for the two samples.[2]

To overcome the problem associated with the much-too-short energy range of the available NM spectra, we propose in the present paper to employ a new method applicable even in these "difficult" cases, but that when applied to "easy" cases, like the one in Fig. 2, gives the same result as the standard approach illustrated above. The alternative procedure we propose to use is as follows:

B1. The linear fit of the pre-edge region is extrapolated forward and subtracted out from the whole spectrum, in this way eliminating the background contribution.

B2. The area, A, under the resulting spectrum is computed.

B3. Each experimental point is divided by A, obtaining what will be called the "normalized spectrum."

With this procedure, the concentration ratio of two samples is directly given by the ratio between the areas of their subtracted spectra. Hence in the case of the two samples Zn_1 and Zn_2, this would be the quantity:

$$\beta = A(Zn_1)/A(Zn_2). \tag{3}$$

Naturally for this method to be reliable, we need to check that β is (largely) independent of the energy interval over which the area A is computed. For this purpose, using the same Zn_1 and Zn_2 XAS data employed before, we have computed A and then β, for various energy intervals for various energy intervals (from a common initial energy, $E_i = 9{,}660$ eV, to different values of the final energy, E_f), getting the results collected in Table 1.

One sees that β is only weakly dependent on the energy interval over which the area integral is computed (the error attributed to β in Table 1 is due to the statistical errors of the original data points and numerical rounding). From the numbers in the table one sees that the average of β is $\langle\beta\rangle = 2.30 \pm 0.04$, where the error is estimated as the dispersion of the four numbers in the last row of the table. Within the margin of error, every value of β is compatible with the concentration ratio α previously determined using the standard procedure, and none of the values of β reported in the table differs by more than 4% from α. We can then conclude from this comparison that the normalization method we propose here to deal with data with a short energy range is fully reliable and can be used for the purposes of the analysis we shall present in the next section.

Third step

There is a small (never larger than 0.5 eV), though visible (because around E_0 the spectrum is very steep) shift in the

[1] As discussed in Stellato et al. (2006), the two spectra are different because different sample preparations lead to different structural atomic arrangements around the Zn binding site.

[2] In fact, at an incoming photon energy of 10.7 keV, the number of counts per data point in a single fluorescence detector element, integrated from 0 keV to infinity, was found to be $T_1 = 183{,}156$ for Zn_1 and $T_2 = 171{,}191$ for Zn_2. Correspondingly the Zn K-fluorescence is $K_1 = 16{,}935$ for Zn_1 and $K_2 = 8{,}130$ for Zn_2. With these numbers one gets $R_1 = T_1/K_1 = 10.82$, $R_2 = T_2/K_2 = 21.056$ and finally $R_2/R_1 = 2.1 \pm 0.2$, in very good agreement with Eq. 2.

Table 1 The areas beneath the subtracted signal computed over different energy intervals. In the bottom line, the resulting Zn concentration ratios are reported

E_f	9,680 eV	9,710 eV	9,760 eV	9,810 eV
Zn_1	2.92	7.19	15.05	22.84
Zn_2	1.26	3.09	6.59	10.12
$\beta \pm \Delta\beta$	2.32 ± 0.02	2.33 ± 0.02	2.28 ± 0.02	2.26 ± 0.02

edge energy among the various samples.[3] To get a feeling about the magnitude of this effect it is useful to recall the following facts.

1. The beam energy resolution with which data were taken is 0.3 eV.
2. The absolute calibration of the energy axis suffers from an uncertainty that also can be estimated to be 0.2 eV.
3. One should not forget that there is a certain ambiguity in the definition of the edge energy itself due to the numerical procedure by which the first derivative of the spectrum is computed and its maximum determined. This numerical step is especially delicate when the XANES region is highly structured, as in our case.

One can estimate the total error on the final determination of the edge energy to be on the order of 0.4 eV. In view of all these considerations, in comparing spectral features of different samples, it is definitely safer to shift the relative position of the various spectra by matching the steep rise of the signal of the various spectra, rather than trying to match their edge energies. Having done that, in the following we will always count and report energies from a common reference point that we (conventionally) identify as the edge energy.

Comparing XANES data

The structure of the XANES region of the spectrum is in principle physically very interesting, as it is fairly sensitive to the electronic structure of the absorber and the symmetry of the local environment around it. Unfortunately, owing to the many very complicated electronic processes contributing (e.g., transitions to bound states, multiple scattering events, etc.), a reliable quantitative way of interpreting this part of the spectrum is still not available, although progress in this direction has been made (Benfatto et al. 1986; Koningsberger and Prins 1988; Lee and Pendry 1975; Rehr and Albers 1990). Despite these difficulties, even a qualitative comparison of the spectra of structurally similar samples can yield valuable information on similarities and differences between local geometries of different compounds (Benfatto et al. 2004; Bianconi et al. 1986) that are not visible in the energy region where single scattering events dominate (i.e., in the EXAFS region).

Since in this paper we want to make use of this observation in order to interpret relative differences among the various spectra as due to different geometries around the S absorber, we need to set up suitable indicators to characterize spectral similarities and differences. We have proceeded to quantify spectral features in two ways. A first crude comparison can be made by simply looking at difference spectra. A second, more refined, analysis consists of trying to fit the interesting (parts of the) spectra of human and synthetic neuromelanins to the spectra of the structurally known model compounds (here cysteine and decarboxytrichochrome C). We now briefly explain in more detail the two approaches.

Difference spectra In order to quantify the difference between the spectra of samples n and m, the simplest thing to do is to consider the quantity

$$\Delta I_{mn} = \sum_{k=N_1}^{N_2} |y_m(E_k) - y_n(E_k)|, \tag{4}$$

where $y_n(E_k)$ is the value of the datum of the subtracted and normalized spectrum of sample n at the (shifted) energy, E_k (see "Data handling") and the sum extends over the desired range of energies for which data are available. Pairs of samples can then be ordered according to the magnitude of this parameter, with the most similar pair attaining the lowest value of ΔI_{nm}.

Fitting analysis The key observation here is that the XAS spectra of samples such as NM on the one hand, or DAC, DEC and DOPEC on the other, where the absorbing atom is present in more than one structure, can in principle be obtained as the sum of (appropriately normalized) model compound spectra, weighted by the percentage of the absorbing atom present in each component (Pickering et al. 1998; Frank and Hodgson 2000). As we have discussed before, in our case the absorbing S atom can exist in two different coordination modes.

The procedure we want to follow then simply consists of trying to reproduce the shape of the spectrum of sample j with a linear combination (with weights p and $1-p$, $0 \leq p \leq 1$) of the spectral data of samples m and n. For a triplet $[j,mn]$ the best value of p is then determined by minimizing the χ^2-like function

[3] The possibility of attributing edge energy differences to different S oxidation states looks implausible. Indeed, systematic studies (Prietzel et al. 2003; George and Gorbaty 1989) on S compounds have shown that samples where S is present in different oxidation states may have the same edge energy, and conversely different geometries with S in the same oxidation state lead to appreciable differences (even on the order of a few eVs) in the edge energy position.

$$R_{[j,mn]} = \sum_{k=1}^{N} \frac{\left[y_j(E_k) - p y_m(E_k) - (1-p) y_n(E_k)\right]^2}{\sigma_j(E_k)^2}, \qquad (5)$$

where N is the number of points included in the fit and $\sigma_j(E_k)$ is the (estimated) statistical error on the normalized data, $y_j(E_k)$. For simplicity in constructing the function $R_{[j,mn]}$ we have assumed that errors are only attributed to the spectral data one is fitting.

As for the evaluation of $\sigma_j(E_k)$, we should observe that there is a certain degree of arbitrariness in estimating the statistical error to be attributed to the normalized data $y(E_k)$. In this paper we have considered two distinct ways of proceeding. The first consists of attributing to the number of measured Auger electrons, $I_{\mathrm{TEY}}(E_k)$ and $I_0(E_k)$, in the TEY detection mode, an error equal to the square root of the number of countings (thus implicitly assuming that countings have a Poisson distribution) and then propagating the errors to the normalized data through the formula yielding $y(E_k)$ in terms of $I_{\mathrm{TEY}}(E_k)$ and $I_0(E_k)$.

As a second alternative, we have considered the possibility of evaluating the errors to be inserted in Eq. 5 by looking at the "typical noise" affecting the measured points. This is done by making reference to the measured spectrum of NM where a pretty large energy range beyond the S K-edge is covered. As we have remarked before, the signal in the EXAFS region does not show any particularly significant structure. Its average value decreases linearly with energy and can be adequately fitted to a straight line. It is then quite natural to identify the sought-for statistical error as the r.m.s. of the fluctuations (around zero) of the subtracted data points belonging to the high energy tail of the spectrum.

The minimization of R is straightforward and gives for the best fit value of p the elementary formula:

$$p_{[j,mn]} = \sum_{k=1}^{N} \frac{\left[y_j(E_k) - y_n(E_k)\right]\left[y_n(E_k) - y_m(E_k)\right]}{\sigma_j(E_k)^2} \times \left[\sum_{k=1}^{N} \frac{\left[y_n(E_k) - y_m(E_k)\right]^2}{\sigma_j(E_k)^2}\right]^{-1}. \qquad (6)$$

Results and discussion

The main purpose of this work is to develop a reliable strategy aimed at understanding the structure and shape of the spectra of natural and synthetic neuromelanins at the S K-edge in terms of the spectral features associated with the characteristic cysteine-like and benzothiazine-like atomic environments surrounding S in the structurally known cysteine and decarboxytrichochrome C model compounds, respectively.

After the spectral data "homogenization" steps described in "Data handling," a first qualitative comparison among the various sets of data we have at our disposal can be made by grouping human and synthetic neuromelanins (i.e., NM and DAC, DEC, DOPEC) spectra on one side (Fig. 3), and the two model compounds (cysteine and decarboxytrichochrome C) plus NM on the other (Fig. 4).

A direct inspection of the four spectra reported in Fig. 3 already shows that, looking at synthetic neuromelanins, there are rather small, but still detectable, differences between DOPEC and DEC, while the differences between these two and DAC are more pronounced. Furthermore, the DOPEC spectrum looks the most similar to that of NM. A more quantitative assessment of these features can be obtained by making use of the indicator introduced in Eq. 4. The results are collected in Table 2. The errors on the numbers reported in the table can be estimated to be less than 1%.

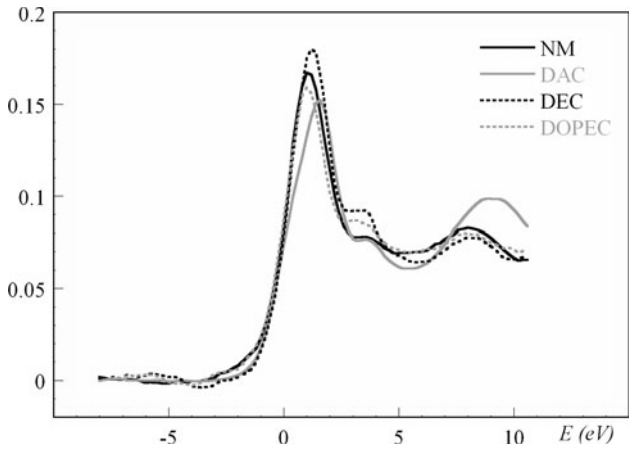

Fig. 3 Comparison among normalized spectral data of human (NM: *black solid line*) and synthetic neuromelanins (DAC: *gray solid line*, DEC: *black dotted line*, DOPEC: *gray dotted line*)

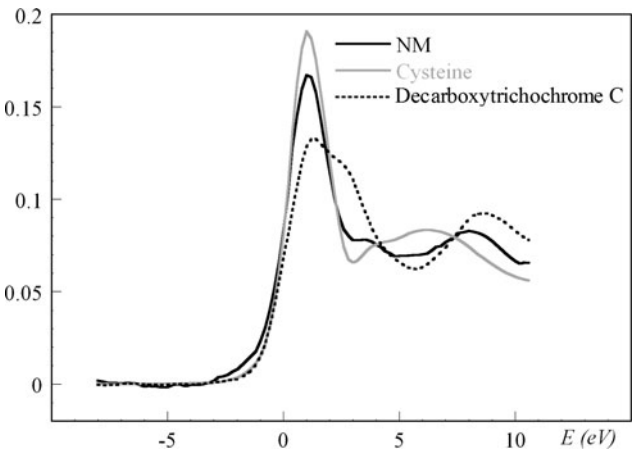

Fig. 4 Comparison among spectral data of human neuromelanin (NM: *black solid line*) and the two model compounds (cysteine: *gray solid line,* decarboxytrichochrome C: *black dotted line*)

Table 2 Spectral differences excluding and including the contribution of the white line

	$E_{Min} = -2.0 - E_{Max}$ = 10.6 eV	Ordering	$E_{Min} = 2.0 - E_{Max}$ = 10.6 eV	Ordering
NM–DOPEC	0.05	1	0.03	1
NM–DEC	0.08	2	0.05	3
NM–DAC	0.14	4	0.09	4
DEC–DOPEC	0.09	3	0.04	2
DAC–DEC	0.15	5	0.10	5
DAC–DOPEC	0.16	6	0.10	5

In computing ΔI_{mn} we have in all cases evaluated the sum up to a unique energy upper limit, namely E_{Max} = 10.6 eV. For E_{Min}, we have taken two different values that correspond to excluding (when $E_{\mathrm{Min}} = 2.0$ eV) or including (when $E_{\mathrm{Min}} = -2.0$ eV) the so-called white-line spectral contribution (i.e., the contribution of the main peak around threshold). Of course the two sets of values of ΔI_{mn} obtained in these two ways are numerically different, but (and this is the interesting point for our discussion) they lead to essentially the same ordering of similarities (see third and fifth columns of Table 2) among the six possible different pairs. In particular we notice that ΔI_{nm} is minimum for the NM–DOPEC pair, followed by the NM–DEC and DEC–DOPEC pairs. As we already noticed, DAC (which is the synthetic neuromelanin obtained by auto-oxidation; see "Experimental methods") shows a spectrum that mostly differs from all the others.

If we now move to Fig. 4, we clearly see that the spectral features of the two model compounds are significantly different (bumps and dips are located at different energies). In Table 3 we make this comparison a bit more compelling by reporting the energy positions of the second maximum (after the main peak) and of the preceding dip of cysteine, decarboxytrichochrome C, and NM. According to the discussion in "Data handling," we present energies counted with respect to the matched position of the edge energies. An error on the order of 0.3 eV should be attributed to the data in the table.

We ascribe the difference in the energy location of the second bump (E_b) and of the preceding dip (E_d) to the different geometrical structure of atoms around S in the two model compounds (see Fig. 1). From the numbers collected in Table 3 we see that the characteristic features of the NM spectrum beyond the white line are somehow in between those displayed by cysteine and decarboxytrichochrome C.

We now want to make more quantitative the previous considerations on the structure of natural and synthetic neuromelanins. This task can be accomplished in an elegant way by using the fitting analysis described at the end of "Comparing XANES data."

We fit the spectrum of NM and synthetic neuromelanins in terms of the spectra of cysteine and decarboxytrichochrome C. In Tables 4 and 5, we collect the results obtained, minimizing the likelihood function of Eq. 5. In column 5 we give, as it is more transparent and customary, the value of R per degree of freedom (R_{dof}) (assuming that the data points included in the computation of R are all statistically independent). With this normalization, a fit should be considered good when R_{dof} is around 1.

The two tables correspond to two different choices of the energy interval over which the sum in Eq. 5 is extended. Table 4 refers to the case where the sum runs over a range of energies that includes the white line. In Table 5 we report the results obtained when, instead, the energy region covering the white line is excluded from the sum. For the reliability of our analysis, it is important to compare these two situations (this is something we also did in Table 2). Actually, as we stressed before, we want to exploit the characteristic features (position and height of bumps and dips) of the structures visible in the spectra of

Table 3 The energy position of the second bump, E_b, and the preceding dip, E_d, in the spectra of NM, cysteine, and decarboxytrichochrome C

Sample	E_d	E_b
Cysteine	3.0	6.0
Tricho	5.8	8.6
NM	4.8	8.0

Table 4 The best fit values of p are shown in columns three and four. These were obtained under the assumption that S in the compound reported in the second column is present in structural environments equal in the percentage of p and $1-p$ to those of cysteine and decarboxytrichochrome C. In column five, the values of the likelihood function per degree of freedom are reported. Data in the energy interval −2.0 to 10.6 eV, which include the main peak, have been used in the sum of Eq. 5

Row	Sample	Cysteine	Tricho	R_{dof}	Figure no.
1	NM	64	36	0.92	5
2	DOPEC	55	45	1.95	6
3	DEC	60	40	1.25	7
4	DAC	19	81	5.24	8

Table 5 The best fit values of p are shown in columns 3 and 4. These were obtained under the assumption that S in the compound reported in the second column is present in structural environments equal in the percentage of p and $1-p$ to those of cysteine and decarboxytrichochrome C. In column five the values of the likelihood function per degree of freedom are reported. Data in the energy interval 2.0–10.6 eV, which exclude the main peak, have been used in the sum of Eq. 5

Row	Sample	Cysteine	Tricho	R_{dof}	Figure no.
1	NM	62	38	0.64	5
2	DOPEC	56	44	1.14	6
3	DEC	48	52	0.98	7
4	DAC	20	80	6.59	8

the model compounds after the main peak, as fingerprints for the presence of either cysteine-like or benzothiazine-like S in the other compounds. Indeed, for the present analysis, no special significance should be attached to the shape of the white lines themselves, which all look very similar. However, since it is not completely obvious how to determine where the peculiar features we are interested in really start along the energy axis, the decision of where to cut the sum in Eq. 5 introduces some degree of ambiguity. In addition, given the rather short energy region over which spectral data extend, it can be statistically dangerous to reduce too significantly the number of points contributing to R. To comply with these conflicting requirements, we decided to perform our analysis both taking into account all data and restricting attention to the part of the spectrum beyond the white line, hoping that the kind of information we desire to extract would not crucially depend on the magnitude of the energy range where the sum in Eq. 5 is extended. Fortunately within the margin of error, the values of p reported in Tables 4 and 5 are fairly consistent.

Furthermore, we have also checked that with our experimental numbers the best fit values of $p_{[j,mn]}$ we obtain are pretty much independent of which of the two methods described above (below Eq. 5) we use to evaluate the statistical errors in Eq. 5.

In Figs. 5, 6, 7, and 8 the spectra resulting from the fits of Table 4 (gray line) and Table 5 (broken line) are shown superimposed on the experimental spectra (solid black line). The fits obtained including or excluding the white line are essentially indistinguishable, except in the case of DEC. This fact is related to higher intensity of the peak of the white line and the more structured shape of the spectrum after the first dip (see Fig. 3) of the DEC spectrum with respect to those of NM and DOPEC.

Physically the most important conclusion one can draw looking at Figs. 5, 6, 7 and 8 and the results in Tables 4 and 5 is that a good fit with the NM spectral data is obtained by assuming that S is present in the sample in the cysteine-like and benzothiazine-like environment at the level of about $p \sim 64\%$ and $1-p \sim 36\%$, respectively,

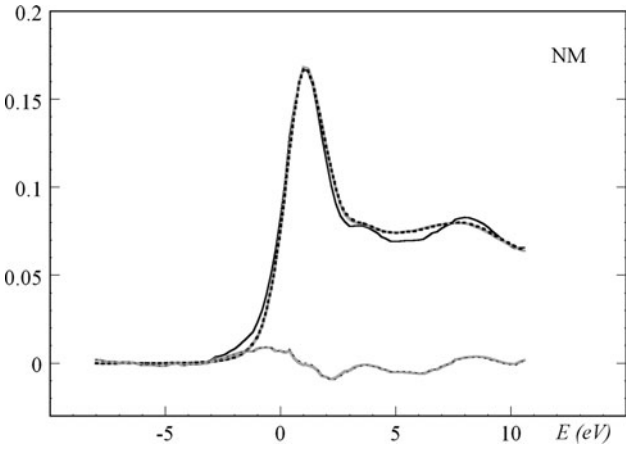

Fig. 5 NM best fit spectra obtained either by including (*gray solid line*, Table 4) or excluding (*black dotted line*, Table 5) the white line contribution are drawn superimposed on normalized experimental data (*black solid line*). Difference spectra are also shown. Energies are counted from the edge energy

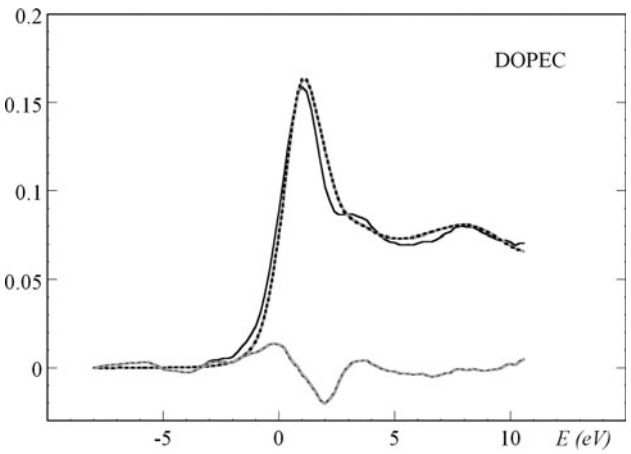

Fig. 6 DOPEC best fit spectra obtained either by including (*gray solid line*, Table 4) or excluding (*black dotted line*, Table 5) the white line contribution are drawn superimposed on normalized experimental data (*black solid line*). Difference spectra are also shown. Energies are counted from the edge energy

with an uncertainty that we can estimate to be $\Delta p \sim 0.05$. This value is obtained using the standard error formula for the fitted parameter p (Eq. 6).

Rather good fits are also obtained for the synthetic neuromelanins, DOPEC and DEC. In the case of DOPEC, the values of p are completely insensitive to whether the points under the white line are included or not in the fit. As we remarked before, this is not the case for DEC. We notice, however, that a value of p very near to those obtained for NM is found when the fit is done over the whole set of spectral data.

The fit to the synthetic neuromelanin DAC data is, in contrast, definitely not very good. This may be put in

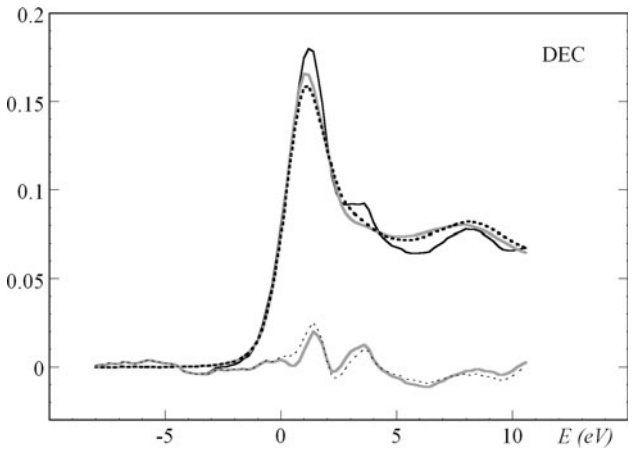

Fig. 7 DEC best fit spectra obtained either by including (*gray solid line*, Table 4) or excluding (*black dotted line*, Table 5) the white line contribution are drawn superimposed on normalized experimental data (*black solid line*). Difference spectra are also shown. Energies are counted from the edge energy

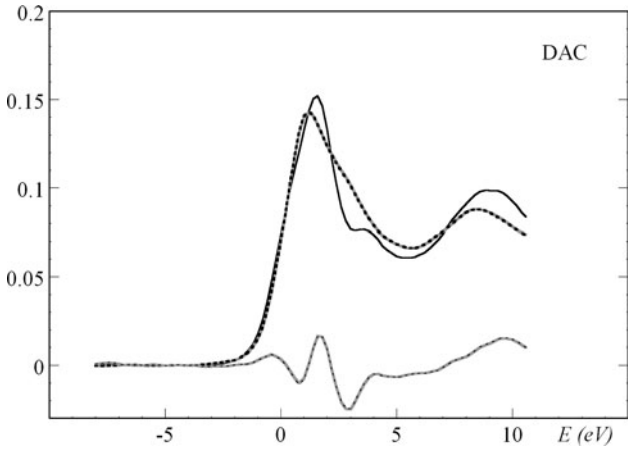

Fig. 8 DAC best fit spectra obtained either by including (*gray solid line*, Table 4) or excluding (*black dotted line*, Table 5) the white line contribution are drawn superimposed on normalized experimental data (*black solid line*). Difference spectra are also shown. Energies are counted from the edge energy

relation to what we indirectly know about its structure on the basis of its preparation process. DAC is, in fact, produced in an auto-oxidation process at the end of which cysteine is removed. It is then not surprising that one cannot fit its spectrum by employing cysteine in addition to decarboxytrichochrome C.

We end this section with the following observation. One could imagine extending the above scheme and consider the possibility of fitting any one of the available spectra in terms of the spectral data of any other pair of compounds. Not much new information, however, can be extracted in this way. The reason is that, for the good fits, the values one obtains for the $p_{j,mn}$ will satisfy the nonlinear relation

$$p_{[j,nm]} = p_{[j,kl]}p_{[k,nm]} + \left(1 - p_{[j,kl]}\right)p_{[l,nm]}, \quad (7)$$

which is a consequence of their physical and mathematical meaning as S concentration percentages.[4] No useful information can be drawn from the cases where the fit is not sufficiently good.

Conclusions

The investigation we have presented in this paper is the first spectroscopic study showing the presence of heterocyclic S of the benzothiazine type in synthetic neuromelanins and natural (human) NM. Although previous studies (Odh et al. 1994; Wakamatsu et al. 2003) reported that chemical degradation of pheomelanins and natural NM generates the typical molecules that derive from benzothiane rings, a direct and nondestructive demonstration of this fact was still missing.

In this paper, we have been able to show that the S environment of NM is most similar to the one present in the synthetic neuromelanins produced by enzymatic oxidation.

Interestingly the presence of different percentages of the S-containing constituents could be quantitatively assessed through the XAS analysis of the S atomic site. We have found that S in NM appears in two different structural coordination modes, namely either bound to a benzothiazine-like ring or present in a cysteine-like environment, in the ratio 64–36 (with an error of 5).

The synthetic neuromelanins obtained by enzymatic oxidation (DEC and DOPEC) are found to be most similar to natural NM, which indicates that NM biosynthesis likely involves enzymatic oxidation.

The whole investigation was possible owing to the extraordinary potentialities offered by the XAS spectroscopy. Although very rarely used in the study of S in biological molecules, XAS has proved to be a very sensitive technique able to identify even small differences among structurally similar compounds.

Acknowledgments We thank G.C. Rossi for many useful discussions and a careful reading of the manuscript. This work was supported by the Brazilian Synchrotron Light Laboratory (LNLS) under proposal DO4B-XAS1-1834. L.Z. was supported by MIUR-FIRB project RBNE03PX83 on "Protein folding and aggregation: metal and biomolecules in protein conformational diseases" and MIUR-PRIN

[4] The interpretation of Eq. 7 is the following. If the spectrum of compound j is fitted in terms of the spectra of compounds m and n, then the resulting value of $p_{[j,mn]}$ should be the same as the one we would obtain multiplying the percentages characterizing the fit of sample j in terms of the compounds k and l, by the values one gets by fitting the spectra of the latter in terms of the spectra of the original compounds m and n. For completeness we notice the formal properties of the $p_{[j,mn]}$ coefficients, $p_{[j,mn]} = 1 - p_{[j,nm]}$, $p_{[j,jm]} = 1$, $p_{[j,jm]} = 0$.

project 2005035582 on "Chemical processes and structural modifications in neurodegeneration." Partial support from MIUR-Italy under PRIN05 Contract is also acknowledged.

References

Backnaes L, Stelling J, Behrens H, Goettlicher J, Mangold S, Verheijen O, Beerkens RGC, Deubenerz J (2008) Dissolution mechanisms of tetravalent sulphur in silicate melts: evidences from sulphur K edge XANES studies on glasses. J Am Ceram Soc 91:721–727. doi:10.1111/j.1551-2916.2007.02044.x

Benfatto M, Natoli CR, Bianconi A, Garcia J, Marcelli A, Fanfoni M, Davoli I (1986) Multiple-scattering regime and higher-order correlations in X-ray-absorption spectra of liquid solutions. Phys Rev B 34:5774–5781. doi:10.1103/PhysRevB.34.5774

Benfatto M, Della Longa S, Wu Z, Qin Y, Pan G, Morante S (2004) The role of Zn in the interplay among Langmuir–Blodgett multilayer and myelin basic protein: a quantitative analysis of XANES spectra. Biophys Chem 110:191–201. doi:10.1016/j.bpc.2004.02.003

Bianconi A, Congiu-Castellano A, Dell'Ariccia M, Giovannelli A, Morante S, Burattini E, Durham PJ (1986) Local Fe site structure in the tense-to-relaxed transition in carp deoxyhemoglobin: a XANES (X-ray absorption near edge structure) study. Proc Natl Acad Sci USA 83:7736–7740. doi:10.1073/pnas.83.20.7736

Bogerts B (1981) A brainstem atlas of catecholaminergic neurons in man, using melanin as natural marker. J Comp Neurol 197:63–80. doi:10.1002/cne.901970106

Bush WD, Garguilo J, Zucca FA, Albertini A, Zecca L, Edwards GS, Nemanich RJ, Simon JD (2006) The surface oxidation potential of human neuromelanin reveals a spherical architecture with a pheomelanin core and a eumelanin surface. Proc Natl Acad Sci USA 103:14785–14789. doi:10.1073/pnas.0604010103

Cheng J, Moss SC, Eisner M (1994) X-ray characterization of melanins-II. Pigment Cell Res 7:263–273. doi:10.1111/j.1600-0749.1994.tb00061.x

Chio S (1977) PhD thesis. University of Houston, Houston

Crippa PR, Wang QJ, Eisner M, Moss SC, Zecca L, Zachack P, Gog T (1996) Structure of human neuromelanin by X-ray diffraction: comparison with synthetics. XVI IPCC Abstr. Pigment Cell Res Suppl 5:72

D'Amato RJ, Lipman ZP, Snyder SH (1986) Selectivity of the parkinsonian neurotoxin MPTP: toxic metabolite MPP+ binds to neuromelanin. Science 231:987–989. doi:10.1126/science.3080808

Ebel H (2004) Quantitative analysis by X-ray induced total electron yield (TEY) compared to XRFA. Powder Diffr 19:90–96. doi:10.1154/1.1649329

Fleet ME (2005) XANES spectroscopy of sulphur in Earth materials. Can Mineral 43:1811–1838. doi:10.2113/gscanmin.43.6.1811

Frank P, Hodgson KO (2000) Defining chemical species in complex environments using K-edge X-ray absorption spectroscopy: vanadium in intact blood cells and Henze solution from the tunicate Ascidia ceratodes. Inorg Chem 39:6018–6027. doi:10.1021/ic000546m

George GN, Gorbaty ML (1989) Sulphur K-edge X-ray absorption spectroscopy of petroleum asphaltenes and model compounds. J Am Chem Soc 111:3182–3186. doi:10.1021/ja00191a012

Gilbert B, Andres R, Perfetti P, Margaritondo G, Rempfer G, De Stasio G (2000) Charging phenomena in PEEM imaging and spectroscopy. Ultramicroscopy 83:129–139. doi:10.1016/S0304-3991(99)00196-5

Graham DG (1979) On the origin and significance of neuromelanin. Arch Pathol Lab Med 103:359–362

Heald SM (1988) In: Koningsberger DC, Prins R (eds) X-ray absorption. Principles, applications, techniques of EXAFS, SEXAFS and XANES. Wiley, New York, pp 87–118

Kastner A, Hirsch EC, Lejeune O, Javoy-Agid F, Rascol O, Agid Y (1992) Is the vulnerability of neurons in the substantia nigra of patients with Parkinson's disease related to their neuromelanin content? J Neurochem 59:1080–1089

Koningsberger DC, Prins R (eds) (1988) X-ray absorption. Principles, applications, techniques of EXAFS, SEXAFS and XANES (and references quoted therein). Wiley, New York

Lee PA, Pendry JB (1975) Theory of the extended X-ray absorption fine structure. Phys Rev B 11:2795–2811

Lindquist NG, Larsson BS, Lydén-Sokolowski A (1988) Autoradiography of [^{14}C] paraquat or [^{14}C] diquat in frogs and mice: accumulation in neuromelanin. Neurosci Lett 93:1–6

Meneghini C, Morante S (1998) The active site structure of tetanus neurotoxin resolved by multiple scattering analysis in X-ray absorption spectroscopy. Biophys J 75:1953–1963

Morante S (2001) The zinc environment in Langmuir–Blodgett phospholipid multi-layers. J Synchrotron Rad 8:975–977

Morante S, González-Iglesias R, Potrich C, Meneghini C, Meyer-Klaucke W, Menestrina G, Gasset M (2004) Inter- and intra-octarepeat Cu(II) site geometries in the prion protein: implication in Cu(II) binding cooperativity and Cu(II)-mediated assemblies. J Biol Chem 279:11753–11759

Odh G, Carstam R, Paulson J, Wittbjer A, Rosengren E, Rorsman H (1994) Neuromelanin of the human substantia nigra: a mixed type melanin. J Neurochem 62:2030–2036

Östergren A, Annas A, Skog K, Lindquist NG, Brittebo EB (2004) Long-term retention of neurotoxic β-carbolines in brain neuromelanin. J Neural Transm 111:141–157

Pickering IJ, Prince RC, Divers T, George GN (1998) Sulfur K-edge X-ray absorption spectroscopy for determining the chemical speciation of sulfur in biological systems. FEBS Lett 441:11–14

Prietzel J, Thieme J, Neuhäusler U, Susini J, Kögel-Knabner I (2003) Speciation of sulphur in soils and soil particles by X-ray spectroscopy. Eur J Soil Science 54:423–433

Ravel B, Newville M (2005) ATHENA, ARTEMIS, HEPHAESTUS: data analysis for X-ray absorption spectroscopy using IFEFFIT. J Synchrotron Rad 12:537–541

Rehr JJ, Albers RC (1990) Scattering-matrix formulation of curved-wave multiple-scattering theory: application to X-ray-absorption fine structure. Phys Rev B 41:8139–8149

Shamoto-Nagai M, Maruyama W, Akao Y, Osawa T, Tribl F, Gerlach M, Zucca FA, Zecca L, Riederer P, Naoi M (2004) Neuromelanin inhibits enzymatic activity of 26S proteasome in human dopaminergic SH-SY5Y cells. J Neural Transm 111:1253–1265

Stellato F, Menestrina G, Dalla Serra M, Potrich C, Tomazzolli R, Meyer-Klaucke W, Morante S (2006) Metal binding in amyloids beta peptides shows both intra- and inter-peptide coordination modes. Eur Biophys J 35:340–351

Stöhr J, Noguera C, Kendelewicz T (1984) Auger and photoelectron contributions to the electron-yield surface extended X-ray absorption fine-structure signal. Phys Rev B 30:5571–5579

Sulzer D, Bogulavsky J, Larsen KE, Behr G, Karatekin E, Kleinman MH, Turro N, Krantz D, Edwards RH, Greene LA, Zecca L (2000) Neuromelanin biosynthesis is driven by excess cytosolic catecholamines not accumulated by synaptic vesicles. Proc Natl Acad Sci USA 97:11869–11874

Vlachos D, Craven AJ, McComb DW (2005) Specimen charging in X-ray absorption spectroscopy: correction of total electron yield data from stabilized zirconia in the energy range 250–915 eV. J Synchrotron Rad 12:224–233

Wakamatsu K, Fujikawa K, Zucca FA, Zecca L, Ito S (2003) The structure of neuromelanin as studied by chemical degradative methods. J Neurochem 86:1015–1023

Wilms H, Rosenstiel P, Sievers J, Deuschl G, Zecca L, Lucius R (2003) Activation of microglia by human neuromelanin is NF-kappaB dependent and involves p38 mitogen-activated protein kinase: implications for Parkinson's disease. FASEB J 17:500–502

Ye T, Lamb LE, Wakamatsu K, Ito S, Simon JD (2003) Ultrafast absorption and photothermal studies of trichochrome C in solution. Photochem Photobiol Sci 2(7):821–823

Zecca L, Mecacci C, Seraglia R, Parati E (1992) The chemical characterization of melanin contained in substantia nigra of human brain. Biochim Biophys Acta 1138:6–10

Zecca L, Pietra R, Goj C, Mecacci C, Radice D, Sabbioni E (1994) Iron and other metals in neuromelanin, substantia nigra and putamen of human brain. J Neurochem 62:1097–1101

Zecca L, Shima T, Stroppolo A, Goj C, Battiston GA, Gerbasi R, Sarna T, Swartz HM (1996) Interaction of neuromelanin and iron in substantia nigra and other areas of human brain. Neuroscience 73:407–415

Zecca L, Costi P, Mecacci C, Ito S, Terreni M, Sonnino S (2000) Interaction of human substantia nigra neuromelanin with lipids and peptides. J Neurochem 74:1758–1765

Zecca L, Fariello R, Riederer P, Sulzer D, Gatti A, Tampellini D (2002) The absolute concentration of nigral neuromelanin, assayed by a new sensitive method, increases throughout the life and is dramatically decreased in Parkinson's disease. FEBS Lett 510:216–220

Zecca L, Zucca FA, Wilms H, Sulzer D (2003) Neuromelanin of the substantia nigra: a neuronal black hole with protective and toxic characteristics. Trends Neurosci 26:578–580

Zecca L, Stroppolo A, Gatti A, Tampellini D, Toscani M, Gallorini M, Giaveri G, Arosio P, Santambrogio P, Fardello RG, Karatekin E, Kleinman MH, Turro N, Hornykiewicz O, Zucca FA (2004) The role of iron and copper molecules in the neuronal vulnerability of locus coeruleus and substantia nigra during aging. Proc Natl Acad Sci USA 101:9843–9848

Zucca FA, Giaveri G, Gallorini M, Alberini A, Toscani M, Pezzoli G, Lucius R, Wilms H, Sulzer D, Ito S, Wakamatsu K, Zecca L (2004) The neuromelanin of human substantia nigra: physiological and pathogenic aspects. Pigment Cell Res 17:610–617